Measurement of the photon dispersion relation in two-dimensional ordered dielectric arrays

W. M. Robertson

Institute for Information Technology, National Research Council Canada, M-50 Montreal Road, Ottawa, Ontario K1A 0R6, Canada

G. Arjavalingam*

IBM Research Division, Thomas J. Watson Research Center, P. O. Box 218, Yorktown Heights, New York 10598

R. D. Meade, K. D. Brommer, A. M. Rappe, and J. D. Joannopoulos

Department of Physics, Massachusetts Institute of Technology, Cambridge, Massachusetts 02139

Received May 12, 1992; revised manuscript received July 13, 1992

We characterize the dispersion relation for electromagnetic-wave propagation in two-dimensional dielectric arrays, using the coherent microwave transient spectroscopy technique. Results of measurements along various symmetry directions of square and triangular lattices are presented. The experimental results are in excellent agreement with theoretical calculations made by using the plane-wave expansion technique. The theoretical calculations predict that transmission via certain modes is forbidden by symmetry, and our experimental results confirm this prediction.

The coherent scattering and interference of electromagnetic radiation in ordered dielectric arrays leads to the formation of frequency intervals in which no photon modes are allowed. The effect is analogous to the existence of gaps in the electron density of states in crystalline solids. By extension of the analogy, the dispersion relation for electromagnetic-wave propagation in an ordered dielectric structure can be described by band theory.[1,2] The subjects of photonic band structure and photonic band gaps have received much attention for both fundamental and practical reasons. The absence of allowed modes within the photonic gap leads to a suppression of spontaneous emission, a fact that could have important consequences for improving the behavior of optical and electronic devices such as semiconductor lasers, solar cells, and bipolar transistors.[1] The suppression of transitions has been observed in Rydberg atoms placed inside a cavity that does not support any modes at the transition frequency.[3] Kurizki and Genack[4] predicted the modification of a number of radiative and dynamical processes in molecular systems owing to the existence of photonic band gaps in periodic structures. Finally, it has also been suggested that localization of electromagnetic radiation should be possible by weak disordering of a periodic dielectric array.[2,5]

The calculation of the photonic band structure by using the plane-wave expansion technique is now well developed and has been applied to a variety of two- and three-dimensional dielectric systems.[6–11] Experimental investigations of photonic band structures have been confined primarily to microwave frequencies because of the ease of fabricating suitable periodic dielectric structures with the appropriate dimensions. Traditional microwave techniques have been used to determine frequencies that define the photonic band gaps, including the demonstration of a three-dimensional system that exhibits a band gap in all propagation directions[12] and the exploration of defect modes within the gaps.[13–14] However, these techniques have not been applied to the determination of the photon dispersion relation. Previously we measured the dispersion relation for electromagnetic-wave propagation along the ⟨10⟩ direction of a two-dimensional dielectric array.[15] The coherent microwave transient spectroscopy (COMITS) technique was employed for these measurements.[16–19] COMITS is based on the radiation and detection of ultrashort electromagnetic transients with optoelectronically pulsed antennas and has been used to characterize the complex dielectric properties of materials across a broad frequency range (15–140 GHz), in a single experiment.

Here we present additional results from our studies of photonic band structure materials, namely, the dispersion relations for propagation along the ⟨11⟩ direction of a square lattice and the ⟨y⟩ direction of a triangular lattice. Our results span the fundamental and the higher band gaps and thus provide a means of directly exploring the validity of the theoretical formalisms. Furthermore, because of the broad frequency coverage, the measurements also elucidate the transition from long wavelengths, where the dielectric array behaves as a continuous medium, to shorter wavelengths, where scattering leads to dispersion and the opening of photonic band gaps.

We chose to explore the photonic band structure of two-dimensional dielectric systems because of the ease of fabricating these samples. However, the COMITS technique is equally capable of measurements in three-dimensional systems. The dielectric structures that we measured con-

0740-3224/93/020322-06$05.00 © 1993 Optical Society of America

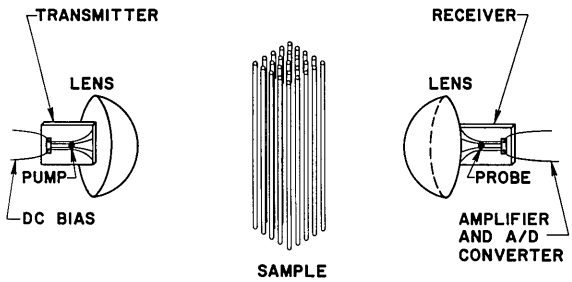

Fig. 1. Experimental setup for coherent microwave transient spectroscopy experiments. The two-dimensional photonic crystal is made of 0.74-mm-diameter, 100-mm-long alumina ceramic rods. Both square and triangular lattices were characterized.

sisted of 100-mm-long alumina ceramic cylinders (diameter of 0.74 ± 0.03 mm) held in a square or triangular array by a machined holder. Alumina ceramic was chosen because of its high dielectric constant and because it exhibits essentially no loss throughout the frequency range of interest. We compare the measured results with the predicted band structure calculated theoretically by using the plane-wave expansion technique.

In order to calculate the electromagnetic frequency spectrum of these dielectric lattices, we have employed the computational techniques described in Refs. 6–11. Briefly, the macroscopic Maxwell's equations can be rearranged to yield the eigenvalue equation

$$\nabla \times \left(\frac{1}{\epsilon(\mathbf{r})}\nabla \times \mathbf{H}\right) - \frac{\omega^2}{c^2}\mathbf{H} = 0. \tag{1}$$

The magnetic field $\mathbf{H}(\mathbf{r})$ can be expressed as a sum of plane waves:

$$\mathbf{H}(\mathbf{r}) = \sum_{\mathbf{G}} \sum_{\lambda=1,2} h_{\mathbf{G},\lambda}\mathbf{e}_\lambda \exp[i(\mathbf{k} + \mathbf{G}) \cdot \mathbf{r}], \tag{2}$$

where $\mathbf{k}$ is in the Brillouin zone, $\mathbf{G}$ is summed over the reciprocal lattice, and $\mathbf{e}_\lambda$ are polarizations orthogonal to $(\mathbf{k} + \mathbf{G})$. This equation could be decoupled as described in Ref. 10. By limiting the size of wave vectors included in this plane-wave expansion, one achieves a finite sum. This eigenvalue equation can now be solved by standard numerical techniques, yielding the normal mode coefficients and frequencies of the electromagnetic modes. Because of the two-dimensional nature of the problems considered, convergence was achieved with a relatively small number of plane waves. We estimate that with 1600 plane waves per polarization the electromagnetic mode frequencies were calculated to better than 1%, although convergence to 2% could be achieved with 400 plane waves. This technique provides a simple and powerful method for solving problems in electrodynamics, which takes full account of the vector nature of the electromagnetic radiation.

The experimental setup for COMITS experiments is shown in Fig. 1. The transmitting and the receiving elements consist of identical coplanar striplines terminated at the radiating end by exponentially tapered flares. The antennas are photolithographically fabricated on silicon on sapphire, and the silicon is subsequently ion implanted to reduce the carrier lifetime to less than 1 ps. Optical pulses (λ = 527 nm, 1.5-ps duration) from a mode-locked pulse compressed and frequency-doubled neodymium-doped yttrium lithium fluoride (Nd:YLF) laser are arranged in a conventional pump–probe configuration. The pump beam, which is focused to a small spot on the silicon between the coplanar striplines, generates a short current transient on the dc-biased transmitter. This pulse propagates down the stripline, spreading in time to ~7 ps because of dispersion and is radiated into free space by the exponentially tapered flare. As is shown in Fig. 1, hemispherical fused silica lenses are used to collimate the transient radiation from the transmitter and to focus the signal, after it passes through the sample, onto the receiver.[18] The time-dependent voltage induced on the receiver is measured, by photoconductive sampling with the probe beam, as a function of the delay between the pump and probe pulses. The induced photocurrent is amplified and detected by a PC-based data-acquisition system. Averaging is performed by adding ~1000 scans with a rapid-scan delay line. The time-domain waveforms are numerically Fourier transformed with a computer. In our experiments the Fourier spectra contain components from 15–140 GHz at intervals of 5 GHz. The 5-GHz frequency resolution is determined by the 200-ps span of the temporal waveforms. Because time-dependent voltage waveforms are measured, phase information is preserved. In addition to its broad frequency spectrum, the radiation is also well polarized (60:1) with the E field lying in the plane of the antenna.[18] A more extensive description of the COMITS technique is given in Refs. 17 and 18.

Measurements on a dielectric array are made by placing the sample in the beam path such that the transient radiation propagates in a plane perpendicular to the axis of the cylinders. The sample is also aligned so that the polarization of the transient radiation is either parallel or perpendicular to the axis of the cylinders. These two polarization orientations permit the characterization of TE and TM modes, respectively, within the photonic crystal. As we demonstrate below, the photon dispersion relation is quite different for the two polarization directions. Furthermore, by symmetry, radiation polarized either parallel or perpendicular to the rod axes preserves this polarization in passing through the array.

The transverse dimensions of the array were always arranged to be larger than the beam size (~3 cm) so that there were no end effects and no interference from the machined holder. The holder consisted of two parallel plates, separated by ~8 cm, each of which is drilled with an identical aligned array of holes. The diameter of each hole was barely larger than that of the alumina cylinders so that the rods could be removed and replaced easily to create arrays with different numbers of rows or to make an array with parallel entrance and exit faces in other symmetry directions. Two holders were made for the experimental results presented here, one for a square array and the other for a triangular array. An overhead view of the triangular and square lattice configurations marked with the measured symmetry directions, lattice constants, and cylinder dimensions is presented in Fig. 2. The lattice constants for the square and triangular arrays were 1.87 and 2.13 mm, respectively, and were designed, based on the results of Refs. 10 and 11, to have a large band gap in the 15–140-GHz frequency range.

Examples of time-domain data are shown in Fig. 3 for

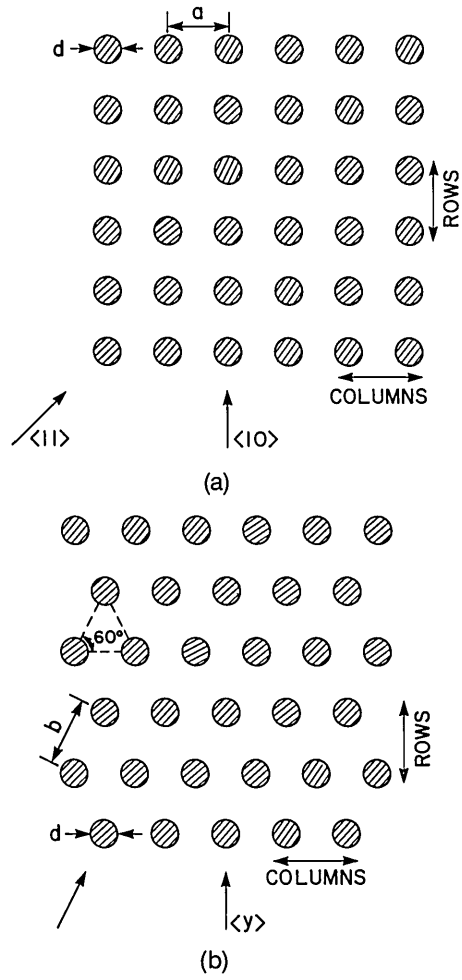

Fig. 2. Schematic diagram of the (a) square and (b) triangular lattice configurations, showing the lattice constants, cylinder diameters, and principal symmetry directions. $d = 0.74$ mm, $a = 1.87$ mm, $b = 2.13$ mm.

propagation along the ⟨11⟩ direction of the square lattice. In Fig. 3(a) we present the measured waveform without any sample, while Figs. 3(b) and 3(c) depict the waveforms recorded with the E field aligned parallel and perpendicular to the rod axes, respectively. In Fig. 4 we present the corresponding amplitude spectra obtained with a numerical Fourier transform. The dashed curves are reference spectra derived from Fig. 3(a), while the filled circles in Figs. 4(a) and 4(b) are calculated from the data in Figs. 3(b) and 3(c), respectively. Although the time-domain data are difficult to interpret, the amplitude spectrum for the E-parallel case [Fig. 4(a)] shows a band gap between 50 and 80 GHz. In the E-perpendicular case [Fig. 4(b)] there is a gap between 85 and 105 GHz. Because of the 200-ps window used for time-domain measurements, the resolution in frequency is 5 GHz, and hence narrow gaps are not necessarily resolved.

Although the amplitude spectra of Fig. 4 give indications of the fundamental and higher photonic band gaps, the dispersion relation can be determined by making use of the phase sensitivity of the COMITS technique. Phase information is preserved in COMITS experiments because the measured signal in the time domain is proportional to the received voltage. The phase data are obtained by determining the complex transmission function of the photonic crystal by measuring time-domain waveforms with and without the sample in the beam path. The time-domain data are Fourier transformed and the transforms divided to produce the complex transmission function of the sample (i.e., transmitted amplitude and phase as a function of frequency). Using the experimentally determined net phase difference, $\phi(f)$, and the thickness of the dielectric array, L, the effective refractive index $n(f)$ of the array can be calculated from

$$n(f) = \frac{c\phi}{2\pi f L} + 1, \tag{3}$$

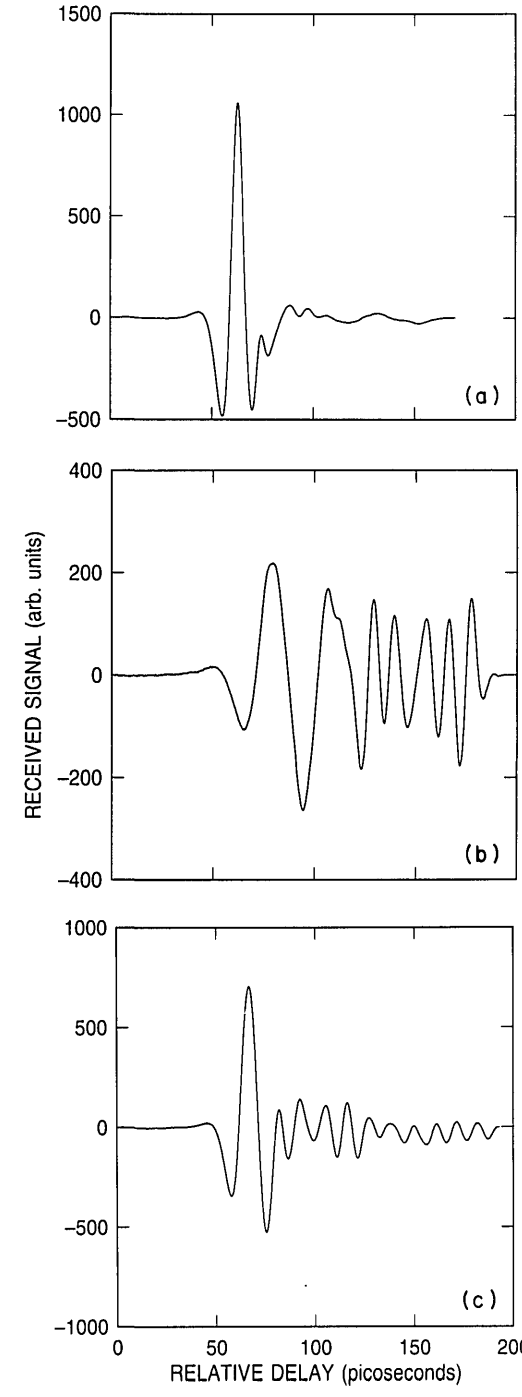

Fig. 3. Time-domain data for propagation through six rows of rods in the ⟨11⟩ direction of the square lattice [Fig. 2(a)]: (a) pulse with no sample; (b) electric field polarized parallel to the rods; (c) electric field polarized perpendicular to the rods.

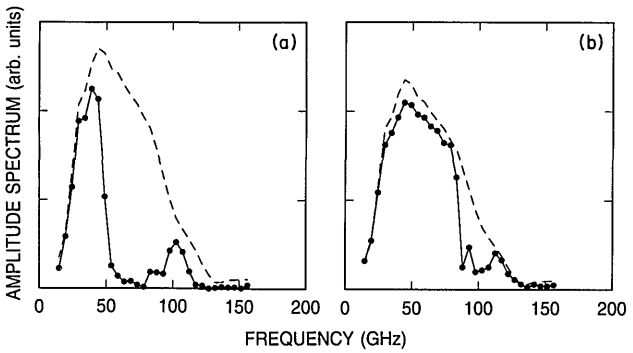

Fig. 4. Amplitude spectra obtained by Fourier transforming the time-domain data shown in Fig. 3. The dashed curves are the amplitude spectrum obtained with no sample in the beam path. The filled circles joined by the solid curves correspond to the cases of (a) the electric field parallel to the rod axes and (b) the electric field perpendicular to the rod axes.

where c is the velocity of light. With the effective index values, the dispersion relation is obtained from

$$k(f) = [2\pi f n(f)]/c. \tag{4}$$

Making use of the phase data to calculate the effective index is a straightforward procedure for the lower modes because there is no phase ambiguity. However, for the higher modes the phase is often too low by factors of $n\pi$ because of the multivalued nature of the arctangent function used in the numerical Fourier transform. The correct phase can be determined by various techniques. A phase jump that occurs in the midst of a monotonically increasing sequence can be found and corrected by inspection. However, if the phase jump occurs across a photonic band gap, i.e., at the zone edge, then such a simple repair is not possible. The true phase in such a case can be found by measuring the phase change resulting from a single row of rods, which is accomplished by determining the transmission function for two photonic crystals whose thicknesses differ by one row. The same information can also be obtained by comparing two or more data sets with different thicknesses and finding the mutually consistent effective index values between them.

Using the phase information associated with the amplitude data shown in Fig. 4, we plot the measured band structure for propagation along the ⟨11⟩ direction of the square lattice as the points in Fig. 5. The curves in the figure are the theoretical band structure for this configuration calculated by the plane-wave expansion technique. The agreement between theory and experiment is excellent for both polarizations. One interesting feature of this study is that our theoretical calculations predict the presence of band 3 in the parallel case (TE mode) and bands 2 and 3 in the perpendicular case (TM modes); however, these bands are not observed experimentally. This result can be understood in terms of simple symmetry arguments, which are discussed below.

Figure 6 shows the amplitude spectra for propagation along the ⟨y⟩ direction of the triangular lattice. For the E-parallel case [Fig. 6(a)] there is a clear band gap between 50 and 65 GHz and the hint of a smaller gap at ~92 GHz. In the E-perpendicular case [Fig. 6(b)] the fundamental gap is suggested by the weak dip in the amplitude spectrum at 75 GHz, while there is a more pronounced minimum at ~100 GHz. Again the features in the amplitude spectrum are more clearly understandable when the associated phase data are used to obtain the dispersion relation. Comparison of the measured and the predicted dispersion relations for propagation along the ⟨y⟩ direction of the triangular lattice are shown in Fig. 7 for the two orthogonal polarization directions. Again the agreement between theory and experiment is generally

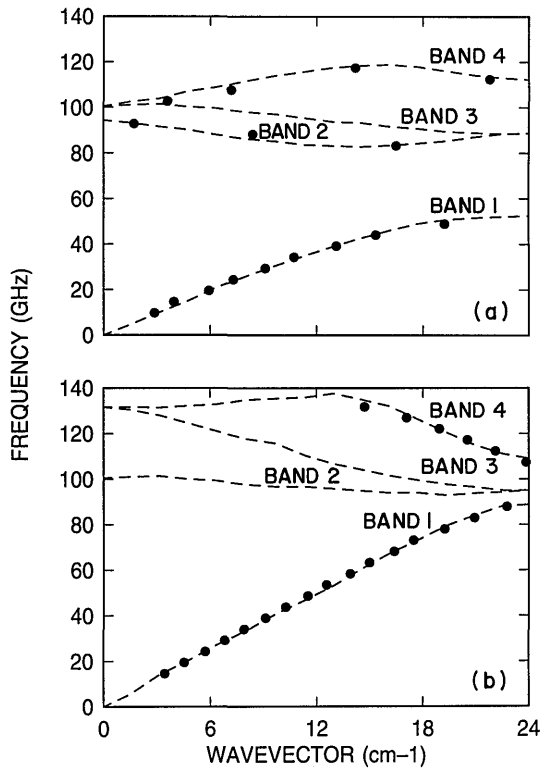

Fig. 5. Band structure for propagation along the ⟨11⟩ direction of the square lattice. The filled circles are the measured values, and the curves are the values calculated theoretically by using the plane wave expansion technique: (a) electric field parallel to rods, TE modes; (b) electric field perpendicular to rods, TM modes.

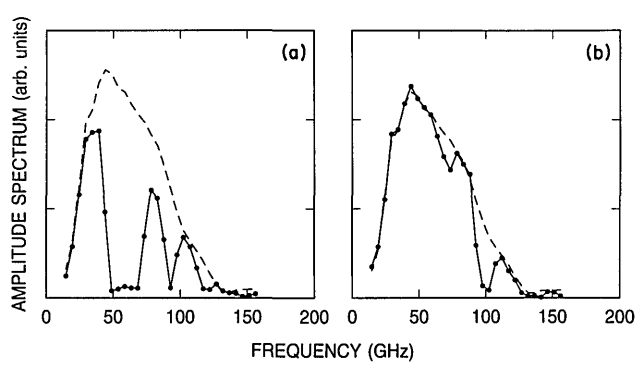

Fig. 6. Amplitude spectra obtained by a numerical Fourier transform of the measured time-domain data for propagation through five rows of rods along the ⟨y⟩ direction of the triangular lattice [Fig. 2(b)]. The dashed curves represent the reference amplitude spectra obtained with no sample in the beam. The filled circles represent the amplitude spectra for (a) the electric field parallel to rods and (b) the electric field perpendicular to rods.

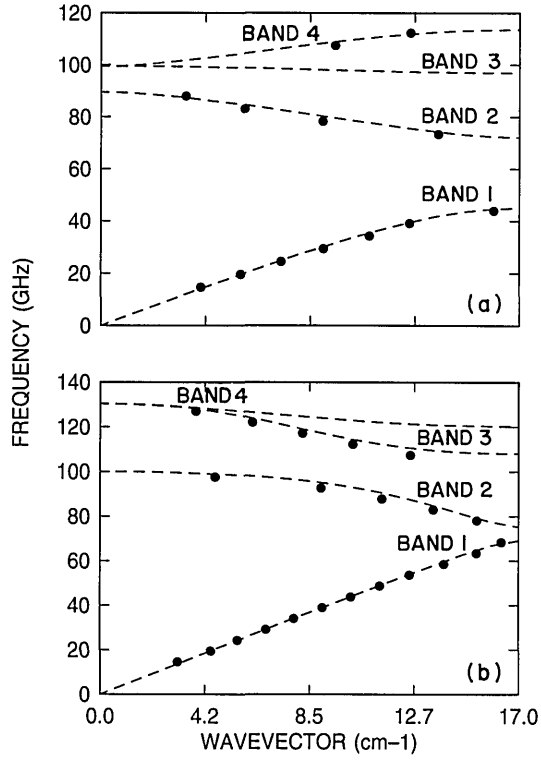

Fig. 7. Band structure for propagation along the ⟨*y*⟩ direction of the triangular lattice. The solid points are the measured values, the lines are the values calculated theoretically by using the plane-wave expansion technique: (a) electric field parallel to rods, TE modes; (b) electric field perpendicular to rods, TM modes.

excellent. In the *E*-parallel case band 3 is not observed, and band 4 is missing in the *E*-perpendicular case.

We now explain the absence of transmission by certain bands that were determined by our theoretical calculations to exist. In essence, excitation of these bands by an incoming plane wave is forbidden by symmetry. In the experiments presented here the dispersion was measured along the symmetry directions of the square and the triangular lattices. These are special directions of the Brillouin zone, which means that the fields associated with the various modes must be either even or odd on reflection through the mirror planes. The mirror planes for propagation along the ⟨11⟩ direction of the square lattice are indicated in Fig. 8. This figure also shows a plot of the calculated field patterns for the first four bands of this situation. All the modes are even under reflection except for band 3, which is odd. This mode is the one that is not observed. In the experiment the incoming plane wave with the *E* field parallel to the rods is even under reflection and thus cannot excite band 3.

In the six cases that we have studied experimentally we have never observed transmission by a band that is of a symmetry opposite to the incident radiation. In only one instance, band 2 in Fig. 5(b), is a mode of the same symmetry as the incident wave not found to transmit radiation. In this case there is some evidence in the amplitude spectrum of transmission at the mode frequency. However, the phase data did not give a reliable value, and hence the point does not appear on the dispersion curve.

For wavelengths much larger than the lattice spacing, i.e., for frequencies well below the fundamental gap, scattering is less important and the dielectric arrays behave as effective media. Because of the ordered nature of the arrays the long-wavelength dielectric constants for the two orthogonal polarizations are given by the absolute Weiner bounds[20]:

$$\epsilon = f_1\epsilon_1 + f_2\epsilon_2, \tag{5}$$

$$\frac{1}{\epsilon} = \frac{f_1}{\epsilon_1} + \frac{f_2}{\epsilon_2}, \tag{6}$$

where f_1 and f_2 are the volume-filling fractions of the two media with dielectric constants ϵ_1 and ϵ_2, respectively. These bounds correspond to the cases of no screening (all dielectric boundaries parallel to the field) and maximum screening (all dielectric boundaries perpendicular to the field) for the *E*-parallel and *E*-perpendicular cases, respectively. Using the dielectric constant of alumina ceramic ($\epsilon = 8.9$) and the cylinder diameters and lattice spacing to calculate the filling fraction, Eqs. (5) and (6) predict microwave refractive indices of 1.41 and 1.06 for the square lattice and 1.37 and 1.05 for the triangular lattice. The lowest-frequency values from the experimental data are 1.47 and 1.11 for the square lattice and 1.38 and 1.09 for the triangular lattice. The dispersion relation for the TM mode should be given exactly by Eq. (5), since the fields are all parallel to the interfaces. The dispersion relation for the TE mode should be given approximately by Eq. (6), since the fields are primarily, although not completely, perpendicular to the interfaces in this case.

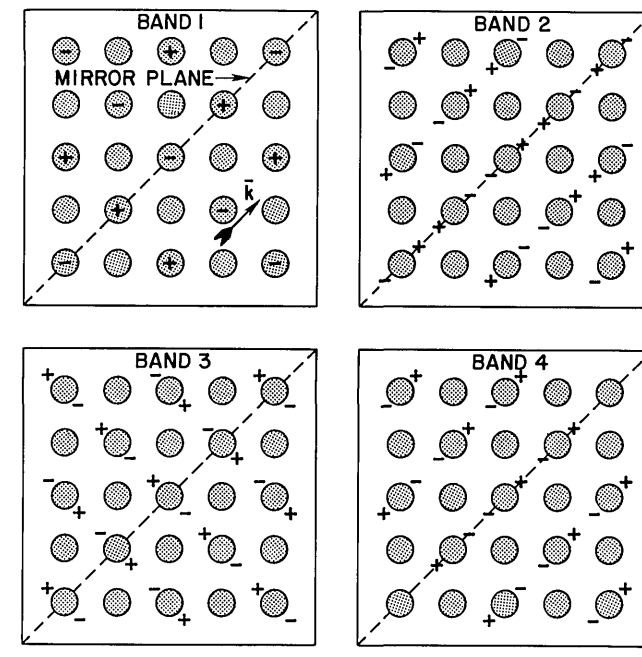

Fig. 8. Symmetries of the electric fields associated with the lowest four photonic bands of the square lattice for propagation along the ⟨11⟩ direction rods. The shaded circles (not to scale) represent the lattice of rods. The states depicted lie at the $k = (1/2, 1/2)$ point of the Brillouin zone. For these modes the electric field is polarized parallel to the rods, and so + (−) indicates regions in which the electric field is oriented into (out of) the page. The modes are even (bands 1, 2, and 4) and odd (band 3) with respect to the mirror plane, shown as the dashed lines.

In summary, we have measured the dispersion relation for electromagnetic-wave propagation in two-dimensional dielectric arrays by using the coherent microwave transient spectroscopy technique. The measured values are in excellent quantitative agreement with theoretical calculations made using the plane-wave expansion technique. However, certain modes that are predicted theoretically are not observed experimentally. We attribute this observation to the fact that our experiments with plane-wave radiation were unable efficiently to excite modes with the opposite symmetry. Thus, although these unobserved modes exist within the crystal, they could not be coupled to in our experimental arrangement. COMITS provides a large frequency bandwidth, which permits measurements on a single system that spans the long-wavelength region, for which the photonic crystal behaves as an effective medium, across the fundamental and higher gaps to short wavelengths, at which there is attenuation caused by multiple scattering.

*Address any correspondence to G. Arjavalingham.

REFERENCES

1. E. Yablonovitch, "Inhibited spontaneous emission in solid-state physics and electronics," Phys. Rev. Lett. **58,** 2059–2063 (1987).
2. S. John, "Strong localization of photons in certain disordered dielectric superlattices," Phys. Rev. Lett. **58,** 2486–2489 (1987).
3. R. G. Hulet, E. S. Hilfer, and D. Kleppner, "Inhibited spontaneous emission by a Rydberg atom," Phys. Rev. Lett. **55,** 2137–2140 (1985).
4. G. Kurizki and A. Z. Genack, "Suppression of molecular interactions in periodic dielectric structures," Phys. Rev. Lett. **61,** 2269–2271 (1988).
5. S. John and R. Rangarajan, "Optimal structures for classical wave localization: an alternative to the Ioffe–Regel criterion," Phys. Rev. B **38,** 10101–10103 (1988).
6. K. M. Leung and Y. F. Liu, "Full vector wave calculation of photonic band structures in face-centered-cubic dielectric media," Phys. Rev. Lett. **65,** 2646–2649 (1990).
7. Z. Zhang and S. Satpathy, "Electromagnetic wave propagation in periodic structures: Bloch wave solution of Maxwell's equations," Phys. Rev. Lett. **65,** 2650–2653 (1990).
8. K. M. Ho, C. T. Chan, and C. M. Soukoulis, "Existence of a photonic gap in periodic dielectric structures," Phys. Rev. Lett. **65,** 3152–3155 (1990).
9. R. D. Meade, K. D. Brommer, A. M. Rappe, and J. D. Joannopoulos, "Existence of a photonic bandgap in two dimensions," Appl. Phys. Lett. **61,** 495–497 (1992).
10. M. Plihal, A. Shambrook, A. A. Maradudin, and P. Sheng, "Two-dimensional photonic band structures," Opt. Commun. **80,** 199–204 (1991).
11. M. Plihal and A. A. Maradudin, "Photonic band structure of two-dimensional systems: the triangular lattice," Phys. Rev. B **44,** 8565–8571 (1991).
12. E. Yablonovitch, T. J. Gmitter, and K. M. Leung, "Photonic band structure: the face-centered-cubic case employing nonspherical atoms," Phys. Rev. Lett. **67,** 2295–2298 (1991).
13. S. L. McCall, P. M. Platzmann, R. Dalichaouch, D. Smith, and S. Schultz, "Microwave propagation in two-dimensional dielectric lattices," Phys. Rev. Lett. **67,** 2017–2020 (1991).
14. E. Yablonovitch, T. J. Gmitter, R. D. Meade, A. M. Rappe, K. D. Brommer, and J. D. Joannopoulos, "Donor and acceptor modes in photonic band structures," Phys. Rev. Lett. **67,** 3380–3383 (1991).
15. W. Robertson, G. Arjavalingam, R. D. Meade, K. D. Brommer, A. M. Rappe, and J. D. Joannopoulos, "Measurement of photonic band structure in a two-dimensional periodic dielectric array," Phys. Rev. Lett. **68,** 2023–2026 (1992).
16. Y. Pastol, G. Arjavalingam, J.-M. Halbout, and G. V. Kopcsay, "Coherent broadband microwave spectroscopy using picosecond optoelectronic antennas," Appl. Phys. Lett. **54,** 307–309 (1989).
17. G. Arjavalingam, Y. Pastol, J.-M. Halbout, and G. V. Kopcsay, "Broad-band microwave measurements with transient radiation from optoelectronically pulsed antennas," IEEE Trans. Microwave Theor. Tech. **38,** 615–621 (1990).
18. Y. Pastol, G. Arjavalingam, G. V. Kopcsay, and J.-M. Halbout, "Dielectric properties of uniaxial crystals measured with optoelectronically generated transient radiation," Appl. Phys. Lett. **55,** 2277–2279 (1989).
19. W. M. Robertson, G. Arjavalingam, and S. L. Shinde, "Microwave dielectric measurements of zirconia–alumina ceramic composites: a test of the Clausius–Mossotti mixture equations," J. Appl. Phys. **70,** 7648–7650 (1991).
20. D. E. Aspnes, "Local-field effects and effective medium theory: a microscopic perspective," Am. J. Phys. **50,** 704–709 (1982).